Shallow geological structures triggered during the M$_w$ 6.4 Meinong earthquake, southwestern Taiwan

Maryline Le Béon[1, *], Mong-Han Huang[2], John Suppe[3, 4], Shiuh-Tsann Huang[5], Erwan Pathier[6], Wen-Jeng Huang[7], Chien-Liang Chen[8], Bénédicte Fruneau[9], Stéphane Baize[10], Kuo-En Ching[11], and Jyr-Ching Hu[3]

[1] *Department of Earth Sciences, National Central University, Jhongli, Taiwan*
[2] *Jet Propulsion Laboratory, California Institute of Technology, Pasadena, California, USA*
[3] *Department of Geosciences, National Taiwan University, Taipei, Taiwan*
[4] *Department of Earth and Atmospheric Sciences, University of Houston, Houston, Texas, USA*
[5] *Exploration and Development Research Institute, Chinese Petroleum Corporation, Miaoli, Taiwan*
[6] *ISTerre, Université Grenoble Alpes, Grenoble, France*
[7] *Active Tectonics Division, Central Geological Survey, MOEA, Chung-Ho, Taiwan*
[8] *Institute of Applied Geology, National Central University, Jhongli, Taiwan*
[9] *Université Paris-Est, LASTIG, IGN, UPEM, Marne-la-Vallée, France*
[10] *Institut de Radioprotection et de Sureté Nucléaire, Fontenay-aux-Roses, France*
[11] *Department of Geomatics, National Cheng-Kung University, Tainan, Taiwan*

ABSTRACT

The Meinong earthquake generated up to ~10 cm surface displacement located 10-35 km W of the epicenter and monitored by InSAR and GPS. In addition to coseismic deformation related to the deep earthquake source, InSAR revealed three sharp surface displacement gradients. One of them is extensional and is inconsistent with the westward interseismic shortening of ~45 mm/yr in this region. The gradient sharpness suggests slip triggering on shallow structures, some of which were not well documented before. To characterize these shallow structures, we investigated potential surface ruptures in the field. Sets of ~NS tension cracks distributed over 25-300 m width, with cumulative extension in the same order as InSAR observations, were found along 5.5 km distance along the extensional gradient and are interpreted as surface rupture. We build two EW regional balanced cross-sections, based on surface geology, subsurface data, and coseismic and interseismic geodetic data. From the Coastal Plain to the E edge of the coseismic deformation area, we propose a series of three active W-dipping back-thrusts: the Houchiali fault, the Napalin-Pitou back-thrust, and the Lungchuan back-thrust. They all root on the 3.5-4.0 km deep Tainan detachment located near the base of the 3-km-thick Gutingkeng mudstone. Further E, the detachment would ramp down to ~7 km depth. Coseismic surface deformation measurements suggest that, in addition to the deeper (15-20 km) main rupture plane, mostly the ramp, the Lungchuan back-thrust, and the Tainan detachment were activated during or right after the earthquake. Local extension is considered as transient deformation at the W edge of the shallow main slip zone.

1. INTRODUCTION

Ground surface ruptures with minor deformation (~0.1-10 cm) are sometimes reported on faults off a moderate to large (M~6-7) earthquake source. This phenomenon has been referred to as triggered slip or coactive faulting. It was observed mostly in California (1968 Borrego Mountain, Allen et al. (1972); 1992 Landers earthquake sequence, Bodin et al. (1994), Price and Sandwell (1998); 1994 Northridge, Cruikshank et al. (1996), Johnson et al. (1996); 2010 El Mayor-Cucapah, Rymer et al. (2010), Wei et al. (2011)), but also elsewhere in the world (1998 Fandoqa, Iran, Berberian et al. (2001); 1999 Izmit, Turkey: Wright et al. (2001); 1999 Chi-Chi, Taiwan: Pathier et al. (2003); 2016 Kumamoto, Japan: Goto et al (2017)). These faint features are not

* *Corresponding author*
  E-mail: mlebeon@gmail.com

straightforward to observe in the field because they require detailed fieldwork away from the main rupture zone to discover very small ground deformation. Therefore, triggered slip likely occurs more often than effectively observed and in a greater variety of tectonic settings.

This study investigates the case of a moderate earthquake, the $M_w6.4$ Meinong earthquake that struck SW Taiwan on February 5, 2016 (Figure 1). The hypocenter was located at 15-20 km depth. Focal mechanisms from various institutions, aftershock distribution, and quick-response source modeling (Huang et al. 2016a; Lee et al. 2016; Central Weather Bureau (www.cwb.gov.tw)) pointed to a NW-SE fault plane dipping 25-30° to the NE for the source of this event. In spite of moderate magnitude and significant depth, this earthquake generated surface deformation of >10 cm monitored by GPS and Interferometric Synthetic Aperture Radar (InSAR) (Huang et al. 2016a), with the largest deformation area unexpectedly located 10 to 35 km W of the epicenter (Figure 2). It showed areas with deformation partitioned by three relatively sharp displacement gradients, oriented N5°E to N20°E, roughly parallel to surficial geological structures (CPC 1989). Joint inversion of seismic waveforms and geodetic data suggests the activation of an additional E-dipping thrust fault W of the epicenter, at shallower depth of 5-10 km (Huang et al. 2016a). Yet, this model is unable to explain all the details in the observed ground surface deformation, implying that additional structures, probably even shallower, must have been activated during this earthquake.

The foothills of the SW Taiwan fold-and-thrust belt accommodate ~4.5 cm/yr EW shortening (Hsu et al. 2009; Lin et al. 2010; Ching et al. 2011; Central Geological Survey 2014; Tsai et al. 2015) within ~40 km distance. However, only few active structures have been identified in this area (Central Geological Survey 2010; Shyu et al. 2016) and their geometry and kinematics remain poorly understood. The deformation gradients revealed in InSAR do not correspond to any previously reported active structure.

The aim of this work is to characterize the shallow structures in the foothills of SW Taiwan and identify those that could have slipped during or right after the earthquake in order to explain the observed coseismic surface deformation. To do so, we first describe surface deformation based on geodesy and post-earthquake field survey of possible triggered ruptures. Then, we build two new regional EW balanced cross-sections, based on surface and subsurface geology, as well as crustal deformation during the Meinong earthquake and the interseismic period. Eventually, we combine coseismic deformation and geological structures to infer which structures were or could have been activated during the earthquake and discuss the mechanisms that could have triggered slip on these faults.

2. GROUND SURFACE DEFORMATION

2.1 Overview of Ground Surface Deformation Observed from Geodesy

Coseismic ground surface deformation was observed from Interferometric Synthetic Aperture Radar (InSAR) using Sentinel-1A (S1A) and ALOS-2 satellites and GPS. Huang et al. (2016a) used ascending and descending S1A interferograms built with images acquired few days before and ~10 days after the earthquake to decompose the line-of-sight (LOS) displacements into horizontal (mostly E-W) and vertical displacements (Figure 2). Coseismic displacements at GPS permanent stations were calculated using positions 4 h before and after the earthquake (Huang et al. 2016a).

NE and SW of the epicenter, coseismic displacements are 2-3 cm towards SW, with slight uplift in the SW and slight subsidence in the NE (Figure 2). In contrast, 10 to 35 km W of the epicenter, from the Lungchuan ridge area to downtown Tainan, coseismic displacements are oriented mostly westward, with 2.1-3.6 cm at GPS stations LNCH, S106, GS30 and CKSV and up to 9 cm from InSAR between Guanmiao town and Lungchuan village. InSAR reveals an area with highest uplift (Figure 2B) of 8-10 cm between Guanmiao and the Lungchuan ridge, with 10.5 cm uplift at GPS station LNCH. On the E side of this area, a significant uplift gradient, oriented N20°E, corresponds to the location of the Lungchuan ridge (Figures 2 and 3). S of the Lungchuan ridge, the uplift gradient follows the Gutingkeng fault trace and becomes sharper, with an uplift change of ~2.6 cm within a very narrow zone (Figure 3, Transect 4). The Lungchuan ridge also corresponds to the E edge of a broad zone where westward displacements increase westward. Transects 2 and 3 display a subtle, but sharp increase in westward displacements located at the Lungchuan ridge crest, suggesting slope instability. N and S of Guanmiao, a 10-km-long and 2-3-km-wide area, oriented N5-10°E, is characterized by horizontal displacements close to zero and by smaller uplift (3-5 cm) relative to surroundings. On the W side, a sharp extensional displacement gradient is observed along the Guanmiao syncline axis, with an increase in westward displacements of 3-5 cm within 300-400 m distance westward (strain ~ 10^{-4}) (Figure 3, Transects 2 and 3). On the E side, ground displacements show a significant compressional gradient, with westward decrease of 7-8 cm in westward displacement and of 2-4 cm in uplift within 1.0-1.5 km (strain ~ -6×10^{-5}) (Figure 3, Transects 1 and 2). Deformation at Guanmiao town itself appears as an anomaly in this pattern, with a gradient in westward displacement of smaller amplitude (3.5-4.0 cm within 0.9 km) that is shifted 1 km to the W compared to N and S of the town (Figure 3, Transect 3).

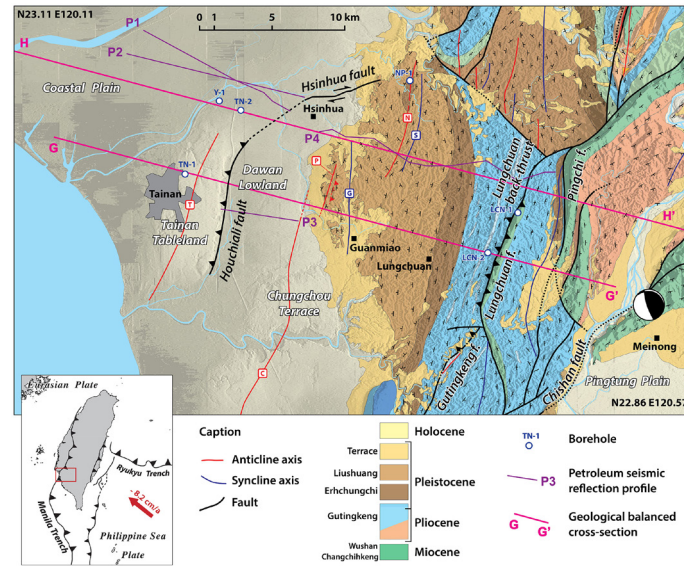### 2.2 Field Survey of Ground Surface Deformation

Fig. 1. Regional geologic map of Tainan area, southwestern Taiwan, modified from Chinese Petroleum Corporation 1:100,000 map, Tainan sheet (1989). Focal mechanism (Huang et al. 2016a) indicates the Meinong earthquake epicenter. Pink lines = balanced cross-section (this study); Purple lines = petroleum seismic reflection profiles from CPC; White dots = boreholes (see text); Fold axes: T = Tainan anticline, C= Chungchou anticline, P= Pitou anticline, N= Napalin anticline, G= Guanmiao syncline, S= Shihtzuchi syncline. Axes of Tainan and Chungchou anticlines are inferred from Pan (1968) Bouguer gravity anomaly map. Inset map shows the background tectonic setting: Taiwan lies at the convergent boundary between the Luzon volcanic arc on the Philippine Sea plate and the continental margin of the Eurasia plate (Suppe 1984). Present-day plate convergence rate is from Hsu et al. (2009) and Tsai et al. (2015).
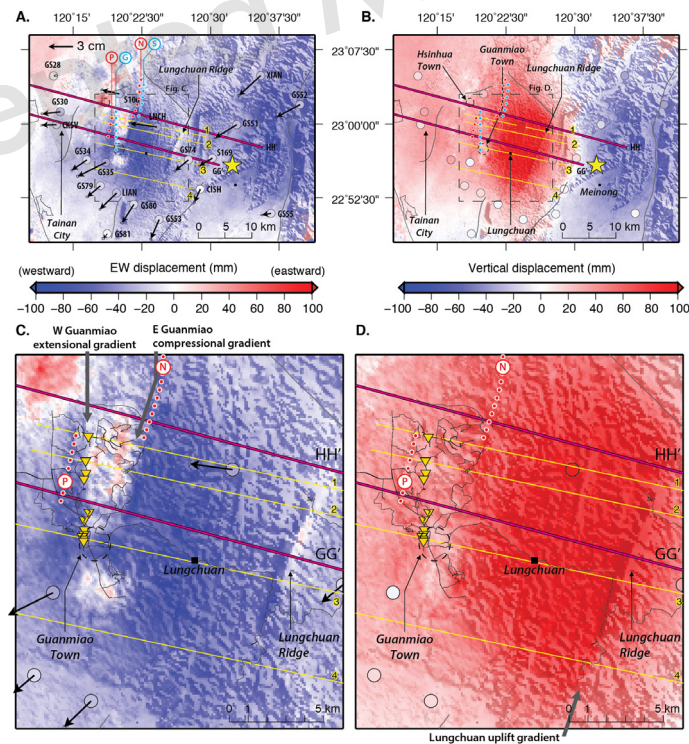

Fig. 2. A. & B. Overview of east-west and vertical coseismic displacements determined from InSAR on Sentinel-1A images and GPS (black arrows)(Huang et al. 2016a). Yellow star shows the Meinong earthquake epicenter. Black lines are reported active faults from Taiwan Central Geological Survey. Yellow and pink lines correspond to transects shown in Fig. 3 and to geological cross-sections, respectively. Red and blue dotted lines indicate Pitou anticline (P), Guanmiao syncline (G), Napalin anticline (N) and Shihtzuchi syncline (S). C. & D. Zooms from A. and B. on the Guanmiao-Lungchuan area. Yellow triangles show sites where ground surface ruptures were found. Black lines shows the path covered during field survey. For convenience, only Pitou and Napalin anticlines are shown.
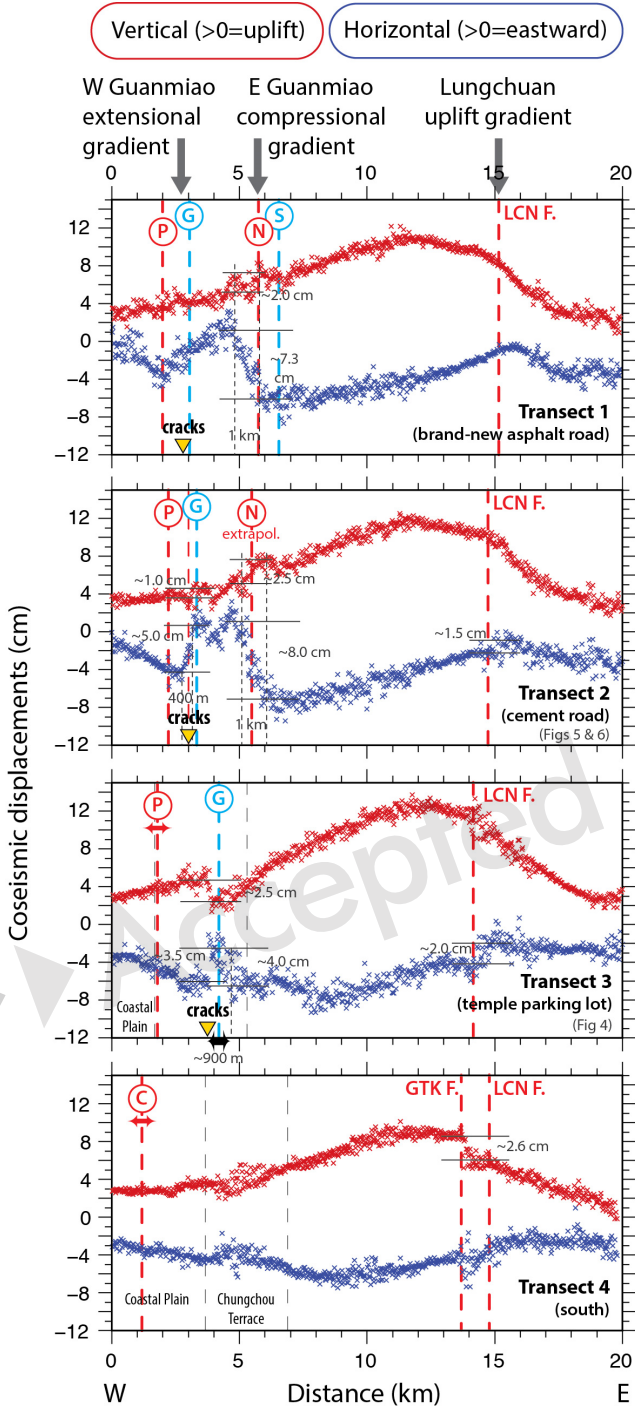
Fig. 3. EW transects of EW and vertical coseismic displacements determined from S1A InSAR (Huang et al. 2016a). See location in Fig. 2. P, N, C = Pitou, Napalin and Chungchou anticlines, G, S = Guanmiao and Shihtzuchi synclines, LCN F. and GTK F. = Lungchuan and Gutingkeng faults (Fig. 1). Black lines and numbers indicate the amplitude and width of displacement gradients.

2.2.1. Survey Strategy, Limitations, and Methodological Aspects

The relatively sharp deformation gradients revealed by InSAR suggested the possibility of surface ruptures that could bring additional information to understand the geological structures that were activated during the Meinong earthquake. The area between downtown Tainan and the Meinong town exhibited multiple kinds of damage related to various mechanisms: collapsed buildings, damaged buildings and infrastructures, liquefaction features, cracks, small-scale landslides, etc (Central Geological Survey 2016; Chung et al. submitted). Because of the limited magnitude of coseismic deformation, offset and aperture along surface ruptures, if any, is expected to be smaller than a few cm. Such features may be hard to distinguish from cracks due to shaking and weaknesses in buildings and infrastructures. Indeed, numerous 1-10-mm-opening tension cracks were found at the tips of bridges, along or across channels, pipes, road ramps and tunnels, and within buildings. The cracks orientation appeared to be guided by the orientation of the infrastructure. Minor tension cracks (<2 mm opening) and fissures across streets also were nearly ubiquitous within the towns of Guanmiao, Hsinhua, and smaller villages, as well as around major road infrastructures. Although some of these features were located along deformation gradients shown in InSAR (Figure 2), the remaining cracks were not, questioning the relationship to geological structures. Similar observations, with slightly higher magnitude though, were made in urban areas after the M_w6.7 1994 Northridge earthquake (Cruikshank et al. 1996; Johnson et al, 1996), the M_w6.0 2014 South Napa earthquake (GEER Association, 2015), and the M_w6.3 2010 Jia-Shian earthquake (Huang, 2013).

To find structurally meaningful cracks corresponding to ground surface ruptures we avoided towns and mainly focused on countryside roads. Careful survey was performed 2 to 7 weeks after the event along significant displacement gradients shown in InSAR, as well as away from them (Figure 2), as a control of our observations. Guanmiao countryside consists mostly in low hills occupied by fields, farms, forest and grasslands, with lush vegetation, and roamed by tiny asphalt, cement or unpaved roads that we explored on foot or on a scooter at low speed. Cracks location was surveyed using a hand-held GPS with 5 m precision. For series of cracks, the cracks relative position was measured using measuring tape with a precision of 2-5 cm. The cracks overall orientation was measured using a compass with a precision of ~2˚. Displacement across the cracks was measured using a ruler with a precision of ≤ 0.5 mm. When possible, the slip vector magnitude and orientation were measured using a compass (± 1˚) and a ruler (± 0.5 mm) (Figures 4 and 6).

2.2.2 Overview of Ground Surface Deformation and Comparison with InSAR Observations

Along the W Guanmiao extensional deformation gradient, sets of significant ~NS tension cracks were found at multiple places from the center of Guanmiao town until ~5.5 km N (Figure 2). Similar cracks were found in SW Guanmiao town (Yi De-Cheng, personal communication, 2016), up to 0.7 km S of the southernmost cracks we found. We could not survey deformation further S. The tension cracks usually appear as a set of 2 to 4 main fractures across paved roads, each with ~5 mm opening in the direction ~N80-110°E and distributed over ~25 to ~60 m wide. In addition, they are accompanied with minor tension cracks and fissures, sometimes over a zone up to 300 m wide. The tension cracks did not propagate into the fields on the sides of the road, probably because deformation was small enough to be diffused within soft granular material such as soils. The total displacement cumulated on the sets of cracks is ~1.5 cm of ~EW extension within ~35 m on the W part of downtown Guanmiao (Figure 4) and up to ~3.1 cm ~N96°E extension within ~300 m at a countryside road 4 km N of Guanmiao (Figures 5 and 6). At first order, these values are consistent with EW displacements observed from InSAR, with 3.0-3.5 cm of EW extension in W Guanmiao and 4.0-5.0 cm of EW extension in the countryside N of Guanmiao (Figure 3, Transects 2 and 3). In Guanmiao town, however, no relative vertical displacement was observed across the cracks, while ~2.5 cm uplift of the W block relative to the E block is observed in InSAR. Field measurements are systematically lower than InSAR estimates, probably because deformation may be distributed over a broader area than that covered by paved surfaces. In addition, small deformation accommodated by tilting over a broad area would not be easily identified in the field. At the northernmost site, where the extensional gradient vanishes (Figure 3, Transect 1), a tension crack with only 2 mm N102°E opening and a minor crack were observed. In areas away from this displacement gradient, only a few tension cracks were found (excluding cracks related to man-made infrastructures). They consisted in isolated minor cracks or fissures, with any orientation and without meaningful geographic location. To summarize, tension cracks were consistently found along ~5.5 km distance on roads going across the W Guanmiao extensional gradient and displayed extension of the same magnitude, at first order, as InSAR observations. We therefore interpret them as a ground surface rupture associated to an active geological structure. Given the width of the deformation zone, ground surface deformation likely reflects an active hinge zone or a buried fault (Huang and Johnson 2010).

The E Guanmiao compressional deformation gradient was also surveyed in detail (Figure 2). However, only isolated minor tension cracks with random location were found. This displacement gradient could be too gentle to result in recognizable deformation in the field (maximum 8 cm over 1 km; Figure 3), and the displacement is possibly related to tilting of the ground surface.

Only a quick survey using a car was done across the N and S tips of the Lungchuan ridge (Figure 2). However, no obvious localized ground deformation (>5 mm amplitude) could be observed.

2.3 Tension Cracks Along the W Guanmiao Extensional Deformation Gradient

In this section, we describe in more details the tension cracks observed at two locations along the W Guanmiao extensional gradient. In W Guanmiao town, a set of ~NS tension cracks could be observed more extensively on a temple parking lot recently paved with asphalt (Figure 4). There, we observed a network of 2 to 3 main tension cracks, oriented N350°E to N12°E and a few minor cracks and fissures. The cracks sharp and distinctive edges provided good markers that allowed measuring slip vectors, oriented N82°E to N103°E with displacements of 3 to 5 mm of the E blocks away from the W blocks. The total extension across this set of cracks is 16 mm in the direction N102°E at the S edge of the parking lot, decreasing to 6 mm in the direction N102°E at the N edge. N of the parking lot, the temple does not exhibit any damage of the pavement nor the walls, probably due to the building strength.

Four km N of downtown Guanmiao, along a road made of ~10-m-long cement tiles, we observed a set of 19 road-perpendicular fractures, including tension cracks, opened joints between cement tiles, and fissures (Figures 5 and 6). On the W part of the site, we found a set of 5 open joints and tension cracks within ~65 m, oriented N337°E to N6°E. The cracks were reactivated from older cracks, but it is hard to conclude if the joints were opened during the earthquake, as the tiles may not have been perfectly adjusted to each other when the road was built. Recent opening of 1-2 mm for each crack and joint is evidenced from sharp cracks within the fine sand that fills the fractures and from a break in the dirt covering the vertical edge of the road. About 100 m further E, a set of 5 open joints and tension crack showed more significant deformation. The central part of the joints, oriented N342°E to N350°E, displayed total separation up to 15 mm, which may result from poor tiles adjustment during road construction and from any subsequent displacements. However, the roadsides were covered with slightly cemented fine sand and silt, displaying recent fractures of smaller aperture (Figure 6A, 6B). The cracks exhibit sharp irregular edges with pieces of cemented sand overhanging above the cracks. Because these micro-overhangs could have been destroyed by rain or any other source of disturbance, they are strong evidence of very recent deformation. The irregular edges of the cracked sand cover lead to slip vectors of 5 mm along N80°E, <2 mm along N72°E, 5 mm along N94°E, and

Fig. 4. Tension cracks on a temple parking lot in Guanmiao town: A. Sketch map, B to E: Field photographs of major cracks where slip vectors could be measured. Site is located along Transect 3 of Figs. 2 and 3.
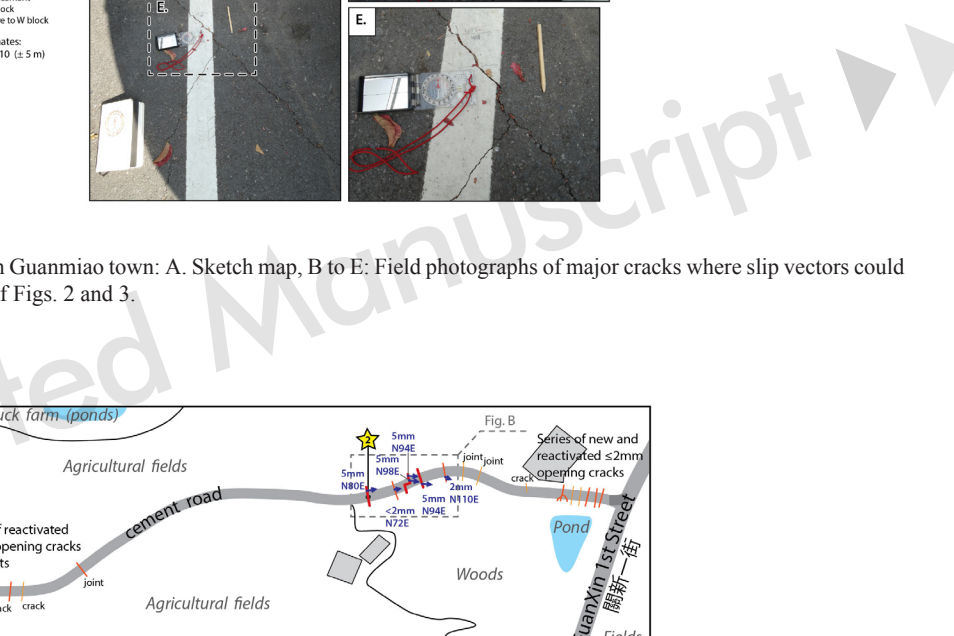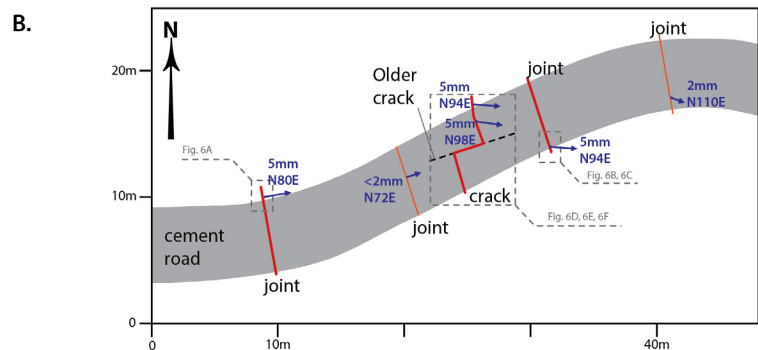

Fig. 5. Sketch maps of tension cracks along a countryside road made from 10-m-long cement tiles, 4.0 km N of Guanmiao town. Panel B focuses on the most significant cracks. Field photographs are presented on Fig. 6. Site is located along Transect 2 of Figs. 2 and 3.

2 mm along N110˚E (Figures 5 and 6C). This site includes a peculiar Z-shape crack (Figures 5 and 6D to 6F), composed of 2 road-perpendicular segments, oriented N339-356˚E, connected by a third segment, N72˚E, that was reactivated from an older crack visible in the central part of the road. Recent deformation could be confidently measured only along the N crack segment: 5 mm along N94˚E to N98˚E. About 50 m further E, a set of 6 new and reactivated tension cracks, oriented N8˚E to N15˚E, displayed ≤2-mm crack-perpendicular (N98˚E to N105˚E) opening. Total extension across the whole site is 31 mm, half of it distributed on 3 open joints and tension crack. The slip vectors average orientation is N96˚E ± 11˚.

3. GEOLOGICAL STRUCTURES IN THE COASTAL PLAIN AND WESTERN FOOTHILLS OF TAINAN REGION

3.1 Surface and Sub-Surface Geological Data and Kinematic Constraints

Strike and dip data from surface geology come from the 1:100,000 geological map of Tainan (Chinese Petroleum Corporation 1989) and from an unpublished local geological map (scale 1:25,000) in the Lungchuan ridge area (Yu et al. 1990), complemented by our own structural measurements in Guanmiao area. We benefit from petroleum seismic reflection profiles P1 to P4 (Figure 1), with depth conversion performed on lines P1 and P2 (Marc et al. 2010). Additional sub-surface constraints come from boreholes TN-1, TN-2 and LCN-2 (Huang et al. 2004), NP-1 (Chung 1968), Y-1 and LCN-1.

We also used coseismic displacements during the Meinong earthquake (InSAR and GPS; Huang et al. 2016a) and interseismic crustal deformation data in order to locate areas where uplift occurs and shortening is consumed. Interseismic velocities come from campaign GPS network from Taiwan Central Geological Survey (e.g. Ching et al. 2011a; Central Geological Survey 2014) during 2002-2014, from precise leveling (e.g. Ching et al. 2011b; Central Geological Survey 2014) during 2012-2015, and from linear regression through position time series of permanent GPS stations of the Institute of Earth Sciences, Academia Sinica, network (e.g. Tsai et al. 2015). Interseismic deformation was also monitored from InSAR using 13 images from the ALOS-1 satellite acquired during the period 2007-2010 (before the 2010 Jia-Shian earthquake; e.g. Huang et al. 2013), along an ascending path, with radar line of sight toward the E with an incidence angle of ~40° (Pathier et al. 2014). Interseismic LOS displacements (Figures 8 and S1) are derived from a time-series analysis based on a small baseline approach
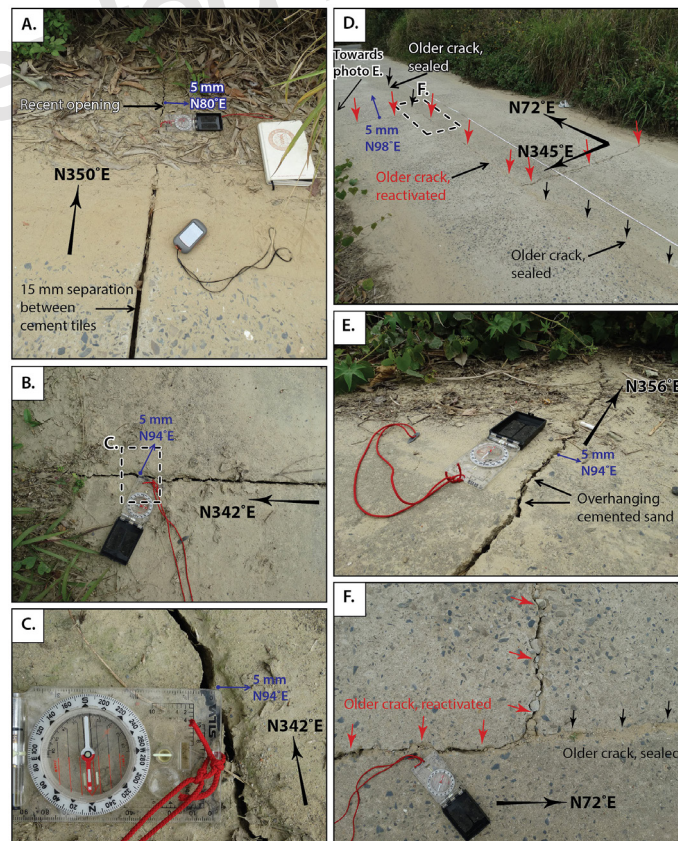

Fig. 6. Field photographs of major cracks found across a cement countryside road, 4 km N of Guanmiao (Fig. 2, Transect 2; Fig. 5B).
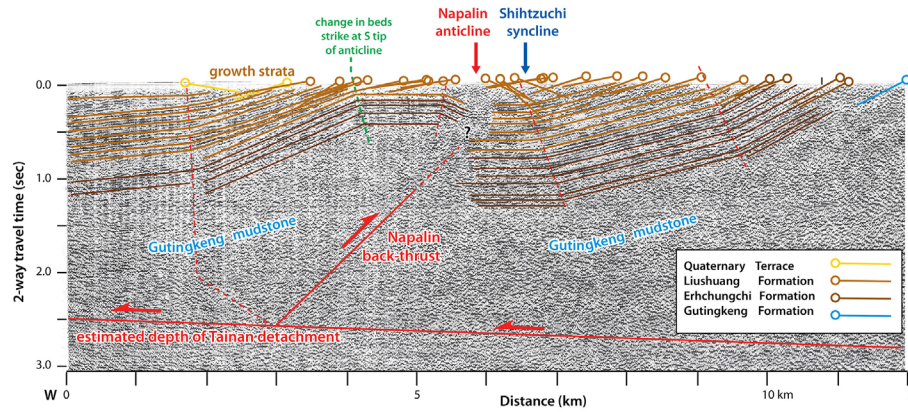
Fig. 7. Interpretation of petroleum seismic reflection profile P4 (location on Fig. 1) across Napalin anticline, based on unmapped profile Sa1 published in Huang et al. (2004).
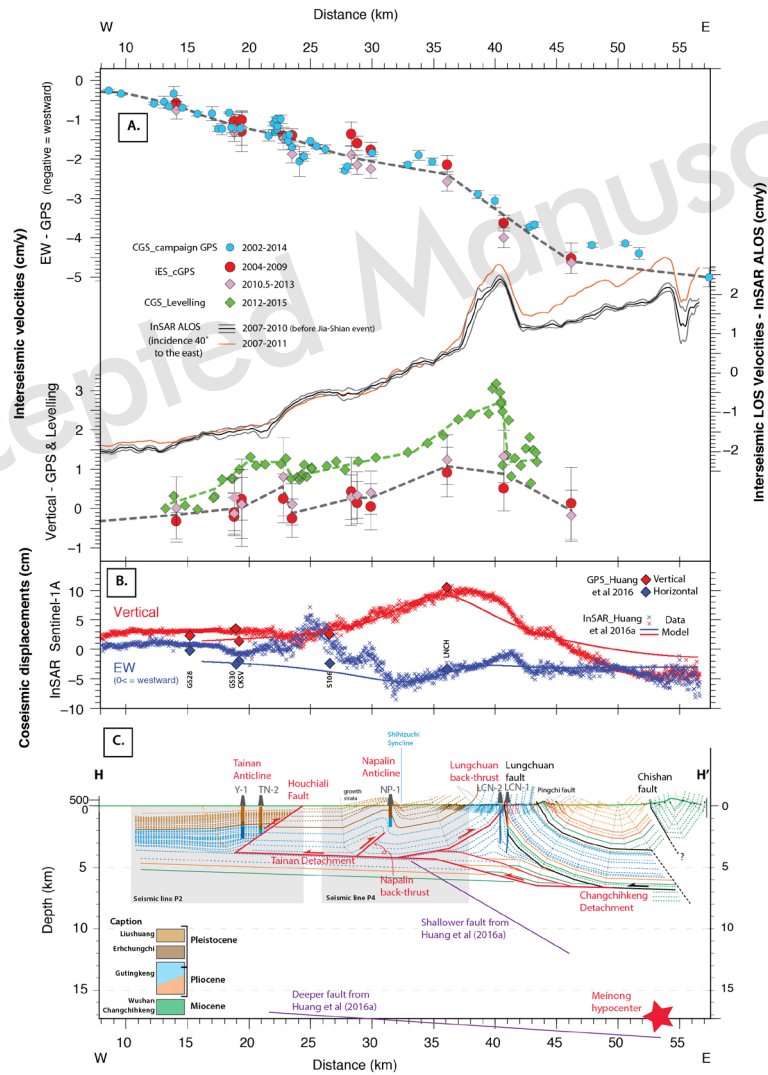

Fig. 8. Transect HH' (Fig. 1): A. Interseismic GPS, levelling and InSAR ALOS-1 line-of-sight velocities (Central Geological Survey 2014; Pathier et al. 2014). B. Meinong coseismic EW and vertical displacements based on Huang et al (2016a) dataset. C. Balanced geological cross-section. Red faults are inferred to have activated during the Meinong earthquake. The earthquake hypocenter is indicated for reference, as well as the deep and shallower faults inferred by Huang et al (2016a) (Purple lines). Note that the shallow dip of Huang et al deep fault (N61°W, dip 15°NE) is apparent.

(NSBAS method, Doin et al. 2011), including atmospheric correction using European Centre for Median-Range Weather Forecast ERAI reanalysis (Doin et al. 2009; Jolivet et al. 2011), DEM errors correction performed before unwrapping (Ducret et al. 2014), and unwrapping following a method similar to Grandin et al. (2012).

3.2 Structural Elements in the Study Area

3.2.1 Within the Coastal Plain

The subsurface structure of Tainan anticline has been previously investigated thanks to depth-converted seismic lines P1 and P2 located at the anticline N tip (Figure 1), combined with InSAR observations and geomorphic analysis. The gently folded reflectors were interpreted as a pure-shear wedge fault-bend-fold growing above a back-thrust that corresponds to the Houchiali fault. The back-thrust roots on a detachment, the Tainan detachment, at a depth of ~3.6 km that was constrained from the deepest deformed reflectors (Marc et al. 2010) and corresponds to the Pliocene Lower Gutingkeng mudstone (Figure 8C). The analysis of InSAR LOS velocities during the aseismic slip period of 1996-1999 (Fruneau et al. 2001; Huang et al. 2009, 2016b) shows that the surface deformation at the Tainan Tableland is consistent with the structural model proposed from the seismic lines N of the tableland (Le Béon et al. 2014). Therefore, a similar pure-shear wedge fault-bend fold model may apply to the Tainan anticline, with a back-thrust that may be steeper along the tableland compared to N of it. The cumulative shortening along the seismic lines was determined to ~800 m only (Marc et al. 2010). The more pronounced topographic expression of the fold to the S and the shallower depth of stratigraphic horizons in borehole TN-1 compared to borehole TN-2 (Figure 1; Huang et al. 2004)
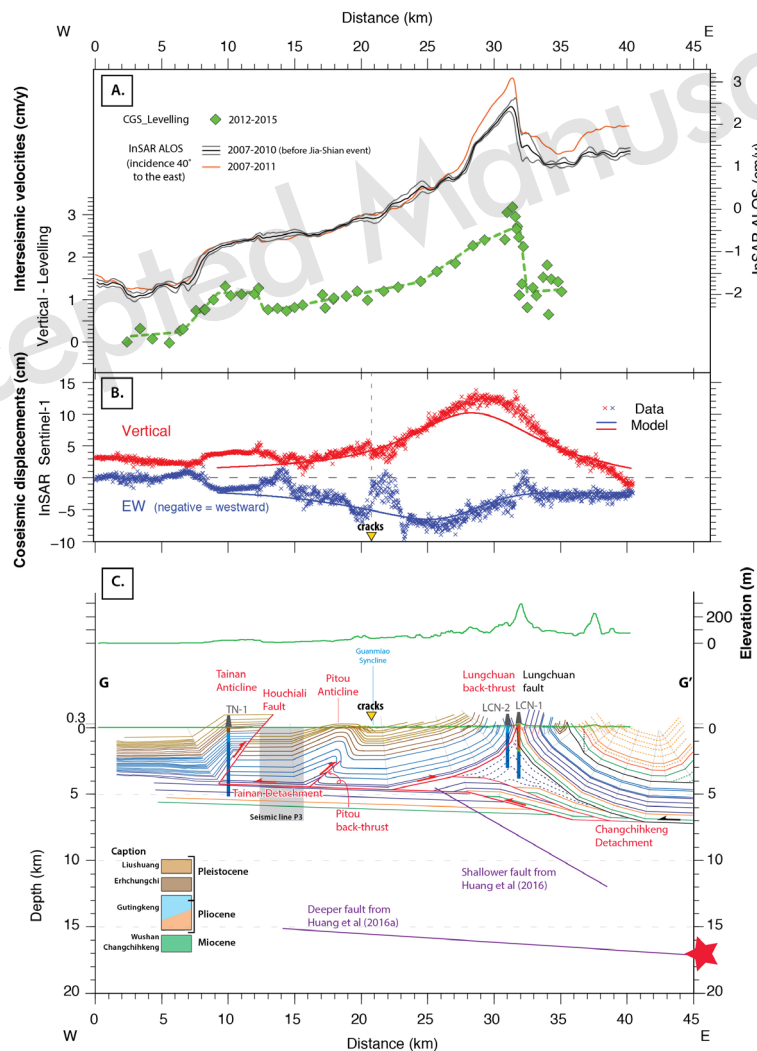

Fig. S1. Transect GG' (Fig. 1): A. Interseismic leveling data and InSAR ALOS-1 line-of-sight velocities (Central Geological Survey 2014; Pathier et al. 2014). B. Meinong coseismic EW and vertical displacements (Huang et al. 2016a). C. Balanced geological cross-section. Red faults are inferred to have activated during the Meinong earthquake. Green line above section shows exaggerated topography.

show that cumulative shortening must be larger to the S. To expand the balanced cross-sections to the E, we use the detachment depth of ~3.6 km and a regional dip for the detachment of 2˚E to account for the geometry of the Chinese continental shelf.

3.2.2 At the Toe of the Western Foothills

On seismic reflection profile P4 (Figures 1 and 7), continuous reflectors from the W tip to ~6 km distance show an asymmetric anticline, the Napalin anticline, with a steep and narrow E limb corresponding to 28-50˚ E-dips in surface geology, and a wide W limb with shallower dips, consistent with surface geology (10-20˚ W). Dip angles appear to be similar for the W limb deeper reflectors, becoming progressively shallower towards the surface within the Pleistocene Liushuang formation, indicative of syntectonic sedimentation above a fold limb that grows by limb rotation (Suppe et al. 2004; Shaw et al. 2005). The deeper reflectors were tentatively mapped as the Pleistocene Erhchungchi formation since it crops out along the Napalin anticline 3 km N of P4 (Figure 1). At ~6 km distance along P4, reflectors are poorly imaged, hampering to conclude on the exact structure of the E limb. The seismic line displays continuous reflectors again from ~6 to ~11 km with increasing W dips towards the E across 2 axial surfaces, and is in agreement with surface geology. Within each kink band, dip angles appear to be similar to each other. The reflection quality drops at the contact between the Erhchungchi formation and the Gutingkeng mudstone.

Because the Napalin anticline is an E-verging fold with the W limb growing by limb rotation, we propose a detachment fold (Epard and Groshong 1995) or a pure-shear fault-related fold (Suppe et al. 2004) growing above a back-thrust, such as a fault-propagation fold (Suppe and Medwedeff 1990) or a tri-shear fold (Hardy and Allmendinger 2009). Because the thickness of sediments displaying good reflection properties is very different across a fairly narrow zone (~1 km) and also because the E-dipping beds in the surface geology are located above the subhorizontal reflectors at depth (Figure 7), we favor a tri-shear fold, with a W limb growing by limb rotation. In cross-section HH', the limited width of the fold compared to the detachment depth requires a fairly steep dip of 37˚ for the back-thrust (Figure 8C). We called this back-thrust the Napalin back-thrust. We cannot exclude the alternative possibility that the fault reaches the surface.

The toe of the Foothills at the latitude of section GG' seems to consist in similar structures, but they are partially imaged. In spite of lower quality imaging, seismic line P3 displays sub-horizontal reflectors down to at least 2.5 sec from the Houchiali fault trace to 2.5 km to the E. Then, from 2.5 km to 3.0 km E of the Houchiali fault trace, the reflectors show W dips down to 2.0 sec. Further E, no reflector

is imaged in the seismic line. Four km further E, between Guanmiao and Hsinhua towns, surface geology shows an anticline, that we called the Pitou anticline (Figures 1 and S1C), with shallow W dips of 2-9˚ and a narrow and steep (28-43˚ W) E limb, similarly to the Napalin anticline E limb. As a simple structural interpretation, we propose that the W dips observed on P3 in Dawan Lowland and at the toe of the foothills connect to each other, which results in a 5-km wide shallow fold limb, similar to the W limb of Napalin anticline (Figure S1C). E of the Pitou anticline, surface geology shows a syncline axis, the Guanmiao syncline, and shallow W-dipping beds, with dip increasing to the E, similarly to section HH' (Figures 7 and 8C). Therefore, the Pitou anticline and Guanmiao syncline, on one hand, and Napalin anticline and Shihtzuchi syncline, on the other hand, appear to be similar structures, en echelon to the W (Figure 1). Therefore, similarly to the Napalin anticline, we expect the Pitou anticline to grow above a back-thrust, that we refer to as the Pitou back-thrust. Based on Bouguer gravity anomalies (Pan 1968), these anticlines likely correspond to the northern continuation of the Chungchou anticline, possibly en echelon to the W relative to Pitou anticline (Figure 1).

3.2.3 In the Lungchuan Ridge Area

Constraints to build this part of the cross-sections come from surface geology, boreholes and crustal deformation. On one hand, surface geology E of the Lungchuan ridge and borehole LCN-1 show that the Miocene Wushan sandstone that forms the ridge has been brought to the surface by an E-dipping thrust fault reaching the surface at the W toe of the ridge (Figures 8C and S1C). Surface geology and borehole data constrain the Lungchuan fault to be sub-vertical from the surface down to 2.0-2.5 km depth, questioning how such fault could be activated as a thrust in the present day. On the other hand, precise leveling and InSAR during the interseismic period show sharp uplift and LOS deformation gradients at the Lungchuan fault trace and Gutingkeng fault trace, with the W side going up relative to the E side (Figures 8A and S1A). Moving W from the Lungchuan fault, leveling shows constant or slightly westward decreasing uplift over ~3 km, then a sharper westward decrease in uplift over ~4 km, to reach a gentle westward decrease until the Houchiali fault ~10 km further W. The sharpness of the displacement gradient strongly suggests the presence of a fault reaching the surface and likely creeping. This higher uplift area is also associated with a higher gradient in EW shortening shown by GPS (Figure 8A). These observations are inconsistent with tectonic activity on the E-dipping Lungchuan fault. However, they could be explained by a back-thrust within the Lower Gutingkeng formation and reaching the surface W of the Lungchuan ridge, possibly at the same location as the E-dipping Lungchuan fault. S of the Lungchuan ridge, the back-thrust would follow the trace

of the Gutingkeng fault. The existence of this back-thrust was previously proposed in Huang et al. (2004) as well. We call this back-thrust the Lungchuan back-thrust. The sedimentary thickness on the hanging wall of the back-thrust is closely similar to the sedimentary thickness in the Coastal Plain, supporting this interpretation. If simply propagating surface dips to depth, the back-thrust consistently flattens at a depth similar to the Tainan detachment, also validating a regional dip of 2˚E for the Mio-Pliocene sediments.

In borehole LCN-1, the Miocene Changchihkeng formation has been reported on top of the Plio-Pleistocene Gutingkeng formation (Figure 8C). Thus, the Lungchuan fault must ramp up from a detachment within the Changchihkeng formation, i.e. deeper than the Tainan detachment. Therefore, a ramp from the Changchihkeng detachment to the Lower Gutingkeng detachment must be located somewhere beneath the Lungchuan ridge area, at depths of 5-7 km.

A vast triangular space remains between the detachment levels, the Lungchuan fault and the Lungchuan back-thrust, with a narrowly pinched upper corner. Boreholes LCN-1 and LCN-2 show that this volume is filled with Gutingkeng mudstone down to 4.2 km depth. Borehole dip data, as reliable as they could be in such homogeneous and low-rigidity rock formation, show fairly consistent dip values of 48-60˚, on either direction. The available space between 4.5 and 7 km depth can be fitted reasonably well by 2 ramps, imbricated under the Lungchuan thrust sheet (Suppe, 1980), involving mainly resistant Changchichkeng and Wushan formations. We propose that the upper part of the triangle consists in Gutingkeng sediments that have been detached from the Wushan sandstone under the stress generated by thrusting of the Lungchuan thrust sheet. This could have been permitted by the high contrast in mechanical properties between the strong Wushan sandstone and Changchihkeng formation, acting as an indenter, and the soft plastic mudstone of Gutingkeng formation, resulting in a narrow detachment fold.

4. DISCUSSION

4.1 Geological Structures Activated During the Meinong Earthquake

4.1.1 Activation of the Ramp and Comparison with the Shallower Fault Inferred from Modeling of Geodetic Data

Following earthquake source modeling of Huang et al. (2016a) based on joint inversion of seismic waveforms and geodetic data, we included for reference the location of the deeper fault where the earthquake nucleated and of the shallower fault on the cross-sections (Figures 8C, S1C). The shallower fault strikes N8˚, dips 30˚W, and ranges from 4.5 to 12 km depth, with most slip between 6 and 9 km depth. Interestingly, it is located at very similar distances along the cross-sections to the ramps inferred independently from ge-

ology with, however, a deeper depth range than the 5-7 km depth of the geology-based ramp and a steeper dip angle (15˚ for the geology-based ramp). For kinematic dislocation inversions, the inferred fault depth or the amount of fault slip is highly dependent of the geodetic data accuracy, as well as of the assumed layered structure computed for Green's functions (Hearn and Bürgmann 2005). More importantly, due to high fluid pressure inferred from the high Vp/Vs ratio underneath the region between Guanmiao and Lungchuan (Huang et al. 2016a), the coseismic deformation at shallower depth here may be inelastic. If we account for inelastic (e.g. plastic) deformation component in the kinematic fault modeling, the inferred fault depth could be shallower. Similarly, the ramps inferred from geology lack precise constraints and could bear a little different attitude. Nonetheless, it seems very likely that the shallower fault inferred by Huang et al. (2016a) could correspond to a ramp at first order similar to the one on cross-sections HH' and GG'. Therefore, this ramp was likely activated during the Meinong earthquake, allowing potential input of westward slip on the Tainan detachment and shallower back-thrusts that root on this detachment.

4.1.2 The Lungchuan Back-Thrust

The Lungchuan back-thrust is the easternmost structure that roots on the Tainan detachment. Based on InSAR and our field exploration, it is not clear if this fault produced surface rupture. Only Transect 4 (Figure 3) shows a displacement discontinuity across the back-thrust that suggests fault slip had reached the surface. Yet, the overall shape of the coseismic uplift transects based on InSAR shows a similar pattern to the leveling transect during the interseismic period, with a gentle eastward increase in uplift, and then a sharp decrease in uplift that corresponds to the Lungchuan back-thrust surface trace. This asymmetry is not predicted in Huang et al. (2016a) model (Figures 8B and S1B), because they did not attempt to model the shallowest fault slip. A contribution to deformation from the Lungchuan back-thrust would produce such E-verging uplift pattern. Therefore, the earthquake likely activated the Lungchuan back-thrust. Regarding uplift budget, since the geology-based ramp is shallower than the model ramp of Huang et al. (2016a), the deficit in uplift due to a shallower ramp may be compensated by slip on the Lungchuan back-thrust.

4.1.3 Extensional and Compressional Gradients Within the Foothills

Along cross-section HH' (Figure 8), the E Guanmiao compressional gradient corresponds to the steep E limb of Napalin anticline, which we proposed to grow above the buried Napalin back-thrust. Activation of this back-thrust would be consistent with consumption of EW shortening at

the anticline E limb. However, while the Napalin anticline is visible in the surface geology until >6 km further N of HH', the compressional gradient vanishes only 2-3 km N of HH' (Figures 1 and 2). In contrast, the Napalin anticline is not observed 1.5 km S of HH', while the compressional gradient is observed until 10 km S. These observations do not favor the Napalin back-thrust as the origin of this deformation gradient. S of HH', the E Guanmiao compressional gradient does not correspond to any change in the surface geology, which consists in shallow ~12˚W dips over a broad area. At greater depth, however, it corresponds, for both sections HH' and GG', to the tip of the wedge between the ramp and the Lungchuan back-thrust, that we argued to have been active during the earthquake. Because of the consistency of surface geology from HH' until 12-14 km further S (Figure 1), this deep structure is expected to exist everywhere beneath the E Guanmiao compressional gradient, so that it appears to be a good candidate to explain this compressional gradient. To get such compression, a significant part of the slip on the ramp must be transferred to the Lungchuan back-thrust, while only a smaller portion propagates westward on the Tainan detachment. As mentioned in section 2.1, at Guanmiao town the E Guanmiao compressional gradient is shifted 1 km to the W compared to N and S of the town (Figure 3, Transect 3). It is very unlikely that geological structures differ beneath Guanmiao town, thus we hypothesize that this shift may be due to a different response of the ground surface in Guanmiao town. The town is densely covered with paved roads and buildings that may make it more resistant to such small deformation, while the surroundings consist in agricultural lands and forest that behave more like a free surface.

Along cross-section GG', ~4.0 cm EW extension is observed across the W Guanmiao extensional gradient, where extensional tension cracks were observed in the field (Figure 2, Transect 2; Figure S1B). It corresponds to the surface trace of the Guanmiao syncline, i.e. the extrapolated trace of the Pitou back-thrust in our interpretation (Figure S1C). Along section HH', extension is very subtle, only ~1.0 cm and no surface cracks were found at this latitude (Figures 2 and 8B). This deformation is still likely related to the Pitou-Guanmiao structure that ends only a few 100 m S. EW extension is however inconsistent with a back-thrust, as well as with a syncline axis and the regional tectonic setting. Instead, this extension may be transient deformation such as elastic pull towards E due to the activation of another nearby structure, which likely is the Lungchuan back-thrust. The steep E limb of the Pitou anticline, that we argued to be controlled by the buried Pitou back-thrust, represents a significant change in the geological structure or a significant weakness zone that could accommodate this eastward elastic pull.

W of the extensional gradient, the Pitou anticline shows absolute westward motion again and higher uplift

relative to Guanmiao area (Figures 2 and S1B). Such displacements may be explained by slip on the deeper fault based on Huang et al. (2016a) model. It is also possible that the Pitou back-thrust was activated by slip on the Tainan detachment and/or potentially promoted by a decrease in normal stress due to local extension.

4.1.4 The Houchiali Fault and the Hsinhua Fault

The InSAR and GPS coseismic displacements (Figures 2, 8B and S1B) show ~2 cm uplift and westward displacements on Tainan Tableland relative to the Coastal Plain and Dawan Lowland. It indicates a minor reactivation of the Houchiali fault and also implies that the Tainan detachment may have slipped as far W as downtown Tainan City during or shortly after the Meinong earthquake.

The ~N70˚E Hsinhua fault is surrounded by a complex surface deformation field (Figures 1 and 2), with patches of eastward displacements on the W part and patches of westward displacements on the E part. The overall orientation of these displacement patches is ~N20˚E, sub-parallel to strike-and-dip data at the toe of the foothills and highly oblique to the Hsinhua fault trace, which was highlighted by liquefaction features during the earthquake (Central Geological Survey 2016). The right-lateral Hsinhua fault slipped during the M6.4 earthquake in 1946 (Bonilla 1975) and appears to act as a tear fault from the toe of the foothills to the Houchiali fault and Tainan anticline. Its role during the Meinong earthquake may have been limited to a weak zone through which over-pressured fluids found their way to the ground surface.

4.2 Relationship to the Earthquake Source and Trigger Mechanism

The shallow structures that activated during the Meinong earthquake are located 10 to 35 km W of the hypocenter and 10-12 km shallower (Figures 8C and S1C), raising the question of the structural or mechanical connections between the two. Huang et al. (2016a) highlighted that the static Coulomb stress change due to slip on their inferred deeper fault did not promote slip of the shallower fault. The depth and dip angle of the ramp inferred in this study are slightly different from the shallower fault inferred in Huang et al. (2016a), but the difference may not be significant enough to switch the static Coulomb stress change to fault failure. We cannot rule out, however, the existence of other structures between the hypocenter and the shallow structures, such as deeper detachment(s) or possible reactivated Paleogene normal faults (e.g. Carena et al 2002; Mouthereau et al. 2001; Mouthereau and Lacombe 2006; Rodriguez-Roa and Wiltschko 2010; Camanni et al 2015), that could have promoted slip on the shallower ramp. Alternatively these shallow structures could be activated dynamically by

seismic waves radiated from the Meinong main fault structure (e.g. Freed 2005).

Earthquake source models based on seismic waveforms converge to a slip patch restricted to the main deep fault close to the epicenter (Lee et al. 2016; Kanamori et al. submitted). Consequently, the shallow faults that slipped beneath the Guanmiao-Lungchuan area did not contribute to seismic waves radiation, so that slip is inferred to be slow or aseismic. High-rate GPS (1 Hz) shows that surface deformation in the Guanmiao-Lungchuan area occurred within 10 minutes after the earthquake (Tung Hsin, personal communication, 2016), so that this aseismic event, which would be equivalent to a M~5.7-5.9 earthquake (Huang et al. 2016a), occurred coseismically or very shortly after the earthquake.

The foothills of SW Taiwan showed cases of aseismic slip prior to the Meinong earthquake, both during interseismic periods and during co- and post-seismic periods. The most obvious example is the creeping Chishan fault that has been progressively deforming a tunnel along National Highway 3, ~18 km S of GPS station LNCH (Central Geological Survey 2014). Within our study area, the sharp gradients in uplift based on leveling and in LOS deformation based on InSAR (Figure 8A) also suggest that the Lungchuan backthrust was creeping during the interseismic period before the Meinong earthquake. Based on InSAR study, transient aseismic slip on the Houchali fault was also inferred during the period 1996-1999 (Huang et al. 2006; 2009) and during 2005-2008 (Huang et al. 2016b). In addition, increased deformation rates across the Houchiali fault were reported during the observation time window that included the 1999 M_w7.6 Chi-Chi earthquake that occurred ~110 km to the NNE (Kao and Chen 2000). Last but not least, the M_w6.3 2010 Jia-Shian earthquake located ~20 km E of Meinong town may have activated the Lungchuan back-thrust and likely other structures (Huang et al. 2013; Lin et al. 2015). The focal mechanism and nucleation depth of the Jia-Shian event are very similar to the Meinong event. Similarly to the Meinong event, seismic waves radiated mainly from a deep slip patch close to the hypocenter (Ching et al. 2011c; Hsu et al. 2011; Huang et al. 2013; Lin et al. 2015). It generated minor cracks around Meinong town (Huang, 2013). ALOS InSAR results show 2-5 cm LOS displacements on the hanging-wall of the Lungchuan back-thrust during a time period covering Jia-Shian earthquake and the following 4 months (Huang et al. 2013). Similarly, longer-term ALOS InSAR observations of interseismic deformation (Pathier et al. 2014) also captured larger velocities on the hanging-wall of the Lungchuan back-thrust during the period 2007-2011 compared to 2007-2010 that does not include the Jia-Shian event (Figures 8A and S1A). The continuous GPS stations maintained by the Institute of Earth Science at Academia Sinica show up to ~5 cm total uplift in Lungchuan, Guanmiao, and Hsinhua area several weeks after the Jia-Shian earthquake, whereas no significant coseismic vertical displacement was observed at these stations. Note that the post-earthquake GPS velocities at these continuous stations are slightly higher after the Jia-Shian event (starting 4 months after the event) compared to before the event (Figure 8A). This was only recorded for the stations near the Guanmiao-Lungchuan area. The CGPS data from stations closer to the Jia-Shian epicenter do not show a significant increase of vertical velocity. We therefore infer that the 2010 Jia-Shian earthquake has temporally increased the slip rate on the shallow structures in the Guanmiao-Lungchuan region.

Long-distance triggering had been observed along the creeping segments of the S San Andreas Fault System after several moderate to large earthquakes (Allen et al. 1972; Bodin et al. 1994), developing the idea that creeping faults can be easily triggered by the passage of seismic waves. Numerical modeling (Du et al. 2003) later supported this hypothesis. The faults mentioned above, on which aseismic slip has been reported or inferred, are located within the Lower Gutingkeng mudstone formation. These soft sediments seem to be rich in fluids, likely over-pressurized, and could explain the existence of active mud volcanoes along active faults in SW Taiwan (Yuan et al. 1987; Sun et al. 2010; Huang et al. 2016a). In the Coastal Plain N of the Tainan anticline, seismic lines P1 and P2 suggest that Lower Gutingkeng formation behaves as a basal pure-shear layer (Marc et al. 2010; Figure 8C). We interpret that the friction in this layer could be too low to accumulate much tectonic strain, so that faults located within this layer are able to slip interseismically and are easier to be triggered by other earthquakes.

5. CONCLUSIONS

In spite of evidence for tectonic activity at different depths, from the shallow upper crust down to 15-20 km depth where the Meinong earthquake nucleated, relatively straightforward relationships could be drawn between sharper gradients in coseismic surface displacement during the Meinong earthquake and shallow geological structures. This allowed us to determine qualitatively which structures were or may have been triggered in the earthquake. These structures are mainly the ramp beneath the Lungchuan ridge, the Lungchuan back-thrust, and the Tainan detachment. The Tainan detachment may have slipped as far W as below the Tainan Tableland, triggering minor slip on the Pitou back-thrust and the Houchiali fault. Testing these inferences by estimating triggered slip on such complex fault geometries, also accounting for the possible inelastic deformation in the Gutingkeng formation, challenges the ability of current numerical modeling techniques.

The structures triggered during the Meinong earthquake are structurally connected, thus faults activation may consist in simple slip partitioning from the ramp and detachment onto the back-thrusts that root on the detachment.

However, the structural connection and triggering mechanism between the shallow structures and the deep source remain to be explained. Retrieving that connection may rely on increased efforts towards seismic instrumentation in order to investigate micro-seismicity and improve the resolution of upper crustal structure imaging techniques.

REFERENCES

Allen, C. R., M. Wyss, J. N. Brune, A. Grantz and R. E. Wallace (1972), Displacements on the Imperial, Superstition Hills and San Andreas faults triggered by the Borrego Mountain earthquake, in The Borrego Mountain Earthquake, U.S. Geol. Surv. Profess. Pap. 787, 87-104

Berberian, M., J. A. Jackson, E. Fielding, B. E. Parsons, K. Priestley, M. Qorashi, M. Talebian, R. Walker, T. J. Wright and C. Baker (2001), The 1998 March 14 Fandoqa earthquake (Mw6.6) in Kerman province, southeast Iran: re-rupture of the 1981 Sirch earthquake fault, triggering of slip on adjacent thrusts and the active tectonics of the Gowk fault zone, Geophys. J. Int., 146, 371-398

Bodin, P., R. Bilham, J. Behr, J. Gomberg and K. W. Hudnut (1994), Slip triggered on southern California fault by the 1992 Joshua Tree, Landers, and Big Bear earthquakes, Bulletin of the Seismological Society of America, 84 (3), 806-816

Bonilla, M. G. (1975), A review of recently active faults in Taiwan, U.S. Geol. Surv. Open File Rep. 75-41, 43 pp.

Carena, S., J. Suppe, and H. Kao (2002), Active detachment of Taiwan illuminated by small earthquakes and its control of first-order topography, Geology, 30 (10), 935-938, doi: 10.1130/0091-7613(2002)

Camanni, G., J. Alvarez-Marron, D. Brown, C. Ayala, Y.-M. Wu, H.-H. Hsieh (2016), The deep structure of south-central Taiwan illuminated by seismic tomography and earthquake hypocenter data, Tectonophysics, 679, 235-245, doi: 10.1016/j.tecto.2015.09.016.

Central Geological Survey (2010), Active fault map of Taiwan (http://fault.moeacgs.gov.tw/UploadFiles/images/500K/C_activefault(A4)_E.jpg)

Central Geological Survey (2014), Report on geodetic monitoring of active faults 2/4 [in Chinese], Ministry of Economic Affairs, Taiwan R.O.C.

Central Geological Survey (2016), Report on the 2016/02/06 Earthquake [in Chinese], Ministry of Economic Affairs, Taiwan R.O.C.

Chinese Petroleum Corporation (1989), Geological map of Tai-Nan, scale 1:100,000, Taiwan Petroleum Exploration Division, Chinese Petroleum Corporation, R.O.C.

Ching, K.-E., R.-J. Rau, K. M. Johnson, J.-C. Lee, and J.-C. Hu (2011a), Present-day kinematics of active mountain building in Taiwan from GPS observations during 1995-2005, J. Geophys. Res., 116, B09405, doi:10.1029/2010JB008058

Ching, K.-E., M.-L. Hsieh, K. M. Johnson, K.-H. Chen, R.-J. Rau, and M. Yang (2011b), Modern vertical deformation rates and mountain building in Taiwan from precise leveling and continuous GPS observations, 2000-2008, J. Geophys. Res., 116, B08406, doi:10.1029/2011JB008242.

Ching, K.-E., K. M. Johnson, R.-J. Rau, R. Y. Chuang, L.-C. Kuo, P.-L. Leu (2011c), Inferred fault geometry and slip distribution of the 2010 Jiashian, Taiwan, earthquake is consistent with a thick-skinned deformation model, Earth and Planetary Science Letters, 301, 78-86, doi:10.1016/j.epsl.2010.10.021

Chung, C. T. (1968), Regional stratigraphic and structural study of the Tainan foothills area, southern Taiwan, Petroleum Geology of Taiwan, 6, p. 15-31

Chung L.-H., R. Y. Chuang, J. B. H. Shyu, M.-H.Huang, K.-M. Yang, K.-E. Ching, M. Le Béon, Y.-H. Lee (submitted to this issue), Shallow crustal structures triggered by the M_L6.6 Meinong earthquake, southwestern Taiwan, from field investigation of surface deformation and damages

Cruikshank, K. M., A. M. Johnson, R. W. Fleming, and R. Jones (1996), Winnetka deformation zone: Surface expression of coactive slip on a blind fault during the Northridge earthquake sequence, California, U.S.

Geol. Surv. Open File Rep. 96- 698, 70 pp.

Covey, M. (1984), Lithofacies analysis and basin reconstruction, Plio-Pleistocene Western Taiwan foredeep, Petroleum Geology of Taiwan, 20, p.53-83

Deffontaines, B., O. Lacombe, J. Angelier, H. T. Chu, F. Mouthereau, C. T. Lee, J. Deramond, J. F. Lee, M. S. Yu, P. M. Liew (1997), Quarternary transfer faulting in the Taiwan Foothills: evidence from a multisource approach, Tectonophys., 274, 61-82.

Doin, M. P., C. Lasserre, G. Peltzer, O. Cavalié, and C. Doubre (2009), Corrections of stratified tropospheric delays in SAR interferometry: Validation with global atmospheric models, *J. Appl. Geophys.*, *69*(1), 35-50, doi:10.1016/j.jappgeo.2009.03.010.

Doin, M. P., F. Lodge, S. Guillaso, R. Jolivet, C. Lasserre, G. Ducret, R. Grandin, E. Pathier, and V. Pinel (2011), Presentation of the small baseline NSBAS processing chain on a case example: the Etna deformation monitoring from 2003 to 2010 using ENVISAT data, in *Proceedings of the Fringe symposium, Frascati, Italy, ESA SP-697*.

Du, W.-X., L. R. Sykes, B. E. Shaw, and C. H. Scholz (2003), Triggered aseismic fault slip from nearby earthquakes, static or dynamic effect?, J. Geophys. Res., 108(B2), 2131, doi:10.1029/2002JB002008.

Ducret, G., M.-P. Doin, R. Grandin, C. Lasserre, and S. Guillaso (2014), DEM Corrections Before Unwrapping in a Small Baseline Strategy for InSAR Time Series Analysis, *IEEE Geosci. Remote Sens. Lett.*, *11*(3), 696-700, doi:10.1109/LGRS.2013.2276040.

Epard, J.-L. and R. H. Groshong (1995), Kinematic model of detachment folding including limb rotation, fixed hinges and layer-parallel strain, Tectonophysics, 247, 85-103

Freed, A. M. (2005), Earthquake triggering by static, dynamic, and post-seismic stress transfer, Annu. Rev. Earth Planet. Sci., 33, 335-67, doi: 10.1146/annurev.earth.33.092203.122505

Fruneau, B., E. Pathier, D. Raymond, B. Deffontaines, C. T. Lee, H. T. Wang, J. Angelier, J. P. Rudant, and C. P. Chang (2001), Uplift of Tainan Tableland (SW Taiwan) revealed by SAR interferometry, Geophysical Research Letters, 28 (16), 3071-3074, doi: 10.1029/2000GL012437

Jolivet, R., R. Grandin, C. Lasserre, M.-P. Doin, and G. Peltzer (2011), Systematic InSAR tropospheric phase delay corrections from global meteorological reanalysis data, *Geophys. Res. Lett.*, *38*(17), L17311, doi:10.1029/2011GL048757.

Geotechnical Extreme Event Reconnaissance (GEER) Association (2014), Geotechnical Engineering Reconnaissance of the August 24, 2014 M6 South Napa Earthquake, Report of the NSF Sponsored GEER Association Team, California Geological Survey, Pacific Earthquake Engineering Research Center and U.S. Geological Survey, GEER-037 (http://www.geerassociation.org/component/geer_reports/?view=geerreports&id=29&layout=default)

Goto, H, H. Tsutsumi, S. Toda, and Y. Kumahara (2017), Geomorphic features of surface ruptures associated with the 2016 Kumamoto earthquake in and around the downtown of Kumamoto City, and implications on triggered slip along active faults, Earth, Planets and Space, 69 (26), doi: 10.1186/s40623-017-0603-9

Grandin, R., M.-P. Doin, L. Bollinger, B. Pinel-Puysségur, G. Ducret, R. Jolivet, and S. N. Sapkota (2012), Long-term growth of the Himalaya inferred from interseismic InSAR measurement, *Geology*, *40*(12), 1059-1062, doi:10.1130/G33154.1.

Hardy, S. and R. W. Allmendinger (2009), Trishear: A review of kinematics, mechanics, and applications, in K. McClay, J. Shaw, and J. Suppe, eds., Thrust fault-related folding: AAPG Memoir 94, p. 1-25.

Hearn, E.H., and R. Bürgmann (2005), The effect of elastic layering on inversions of GPS data for earthquake slip and stress changes. *Bull. Seism. Soc. Am.*, *95*, 1637-1653.

Hsu, Y.-J., S.-B. Yu, M. Simons, L.-C. Kuo, and H.-Y. Chen (2009), Interseismic crustal deformation in the Taiwan plate boundary zone revealed by GPS observations, seismicity, and earthquake focal mechanisms, Tectonophysics, 479, 4-18, doi:10.1016/j.tecto.2008.11.016.

Hsu, Y.-J., S.-B. Yu, L.-C. Kuo, Y.-C. Tsai and H.-Y. Chen (2011), Coseismic deformation of the 2010 Jiashian, Taiwan earthquake and implications for fault activities in southwestern Taiwan, Tectonophysics, 502, 328-335, doi:10.1016/j.tecto.2011.02.005

Huang, I.-J. (2013), Study of the relationship between surface rupture and faulting in relation to Jiashian earthquake, MS Thesis, 315 pp, National Central University, Taoyuan [in Chinese].

Huang, M.-H., J.-C. Hu, C.-S. Hsieh, K.-E. Ching, R.-J. Rau, E. Pathier, B. Fruneau, and B. Deffontaines (2006), A growing structure near the deformation front in SW Taiwan as deduced from SAR interferometry and geodetic observation, Geophys. Res. Lett., 33, L12305, doi:10.1029/2005GL025613.

Huang, M.-H., J.-C. Hu, C.-S. Hsieh, K.-E. Ching, R.-J. Rau, and E. Pathier (2009), Active deformation of Tainan Tableland of southwestern Taiwan based on geodetic measurements and SAR interferometry. *Tectonophysics*, 466, 322-334.

Huang, M.-H., D. Dreger, R. Bürgmann, S.-H. Yoo, and M. Hashimoto (2013), Joint inversion of seismic and geodetic data for the source of the 2010 March 4, Mw 6.3 Jia-Shian, SW Taiwan, earthquake, Geophys. J. Int., 193, 1608-1626.

Huang, M.-H., H. Tung, E. J. Fielding, H.-H. Huang, C.

Liang, C. Huang, and J.-C. Hu (2016a), Multiple fault slip triggered above the 2016 Mw 6.4 Mei-Nong earthquake in Taiwan, Geophys. Res. Lett., 43, doi:10.1002/2016GL069351.

Huang, M.-H., Bürgmann, R., and Hu, J.-C. (2016b), Fifteen years of surface deformation in Western Taiwan: Insight from SAR interferometry, Tectonophysics, doi: 10.1016/j.tecto.2016.02.021

Huang, S.-T., K.-M. Yang, J.-H. Hung, J.-C. Wu, H.-H. Ting, W.-W. Mei, S.-H. Hsu and M. Lee (2004), Deformation front development at the northeast margin of the Tainan basin, Tainan-Kaohsiung area, Taiwan, Marine Geophysical Researches, 25, p. 139-156, doi:10.1007/s11001-005-0739-z

Huang, W.-J., and A. M. Johnson (2010), Quantitative description and analysis of earthquake-induced deformation zones along strike-slip and dip-slip faults, J. Geophys. Res., 115, B03408, doi:10.1029/2009JB006361.

Johnson, A. M., R. W. Fleming, K. M. Cruikshank, and R. F. Packard (1996), Coactive fault of the Northridge earthquake- Granada Hills area, California, U.S. Geol. Surv. Open File Rep. 96- 523, 66 pp.

Kanamori, H. et al., A strong-motion hot spot of the 2016 Meinong, Taiwan, earthquake (Mw=6.4), submitted to this issue.

Kao, H., and W.-P. Chen (2000), The Chi-Chi earthquake sequence: Active, out-of-sequence thrust faulting in Taiwan, Science, 288, 2346-2349, doi:10.1126/ science.288.5475.2346.

Le Béon, M., O. Marc, M.-H. Huang, S.-T. Huang, J. Suppe, R.-F. Chen, Deep structure and deformation history of the rapidly growing Tainan anticline, southwestern Taiwan, Geodynamics and Environment in East Asia International Conference & 7th Taiwan-France Earth Science Symposium, Hualien, Taiwan, November 12-18 2014, Abstract.

Lee, S.-J., T.-Y. Yeh and Y.-Y. Lin (2016), Anomalously Large Ground Motion in the 2016 M_L 6.6 Meinong, Taiwan, Earthquake: A Synergy Effect of Source Rupture and Site Amplification, Seismological Research Letters, 87 (6), doi: 10.1785/0220160082

Lin, K.-C., J.-C. Hu, K.-E. Ching, J. Angelier, R.-J. Rau, S.-B. Yu, C.-H. Tsai, T.-C. Shin, and M.-H. Huang (2010), GPS crustal deformation, strain rate, and seismic activity after the 1999 Chi-Chi earthquake in Taiwan, J. Geophys. Res., 115, B07404, doi:10.1029/2009JB006417.

Lin, K.-C., B. Delouis, J.-C. Hu, L.-M. Nocquet, and L. Mozziconacci (2015), Reassessing the complexity of the rupture of the 2010 Jia-Shian Earthquake (Mw 6.2) in Southwestern Taiwan by inverting jointly teleseismic, strong-motion and CGPS data, *Tectonophysics*, doi: 10.1016/j.tecto.2015.09.015

Marc, O., J. Suppe, S. Huang, M. Le Béon, M. H. Huang, J. C. Hu, Deep structure and deformation history of the rapidly growing Tainan anticline, southwestern Taiwan, AGU Fall Meeting, San Francisco, USA, December 13-17 2010, Abstract.

Mouthereau, F., O. Lacombe, B. Deffontaines, J. Angelier, and S. Brusset (2001), Deformation history of the southwestern Taiwan foreland thrust belt: insights from tectono-sedimentary analyses and balanced cross-sections, *Tectonophysics*, 333 (1-2), 293-318, doi: 10.1016/S0040-1951(00)00280-8

Mouthereau, F. and O. Lacombe (2006), Inversion of the Paleogene Chinese continental margin and thick-skinned deformation in the Western Foreland of Taiwan, *Journal of Structural Geology*, 28 (11), 1977-1993, doi: 10.1016/j.jsg.2006.08.007

Pan, Y. S. (1968), Interpretation and seismic coordination of the Bouguer gravity anomalies obtained in southwestern Taiwan, Petroleum Geology of Taiwan, 6, p.197-208

Pathier, E., B. Fruneau, B. Deffontaines, J. Angelier, C.-P. Chang, S.-B. Yu, and C.-T. Lee (2003), Coseismic displacements of the footwall of the Chelungpu fault caused by the 1999, Taiwan, Chi-Chi earthquake from InSAR and GPS data., *Earth and Planetary Science Letters*, *212*(1-2), 73-88.

Pathier E., B. Fruneau, M-P. Doin, Y-T. Liao, J.-C. Hu, Champenois (2014), What are the tectonic structures accommodating the present-day tectonic deformation in South-Western Taiwan? A new interpretation from ALOS-1 InSAR and GPS interseismic measurements. Geodynamics and Environment in East-Asia: 7th France-Taiwan Earth Sciences Symposium. 12-15 novembre 2014, Hualien, Taiwan

Price, E. J. and D. T. Sandwell (1998), Small-scale deformations associated with the 1992 Landers, California, earthquake mapped by synthetic aperture radar interferometry phase gradients, J. Geophys. Res., 103 (B11), 27,001-27,016

Rodriguez-Roa, F. A. and D. V. Wiltschko (2010), Thrust belt architecture of the central and southern Western Foothills of Taiwan, *Geological Society, London, Special Publications*, 348, 137-168, doi:10.1144/SP348.8

Rymer, M. J., J. A. Treiman, K. J. Kendrick, J. J. Lienkaemper, R. J. Weldon, R. Bilham, M. Wei, E. J. Fielding, J. L. Hernandez, B. P. E. Olson, P. J. Irvine, N. Knepprath, R. R. Sickler, X. Tong, and M. E. Siem (2010), Triggered surface slips in southern California associated with the 2010 El Mayor-Cucapah, Baja California, Mexico, earthquake, U.S. Geol. Surv. Open File Rep. 2010-1333, 72 pp.

Shaw, J. H., C. Connors, and J. Suppe (2005), Seismic interpretation of contractional fault-related folds, An AAPG Seismic Atlas: AAPG Studies in Geology, 53, 156 pp.

Shyu, J. B. H., Y. R. Chuang, Y. L. Chen, Y. R. Lee, and C. T. Cheng (2016), A new on-land seismogenic structure

source database from the Taiwan Earthquake Model (TEM) project for seismic hazard analysis of Taiwan, Terr. Atmos. Ocean. Sci., 27, 311-323, doi: 10.3319/TAO.2015.11.27.02(TEM)

Sun, C.-H, S.-C. Chang, C.-L. Kuo, J.-C. Wu, P.-H. Shao and J.-N. Oung (2010), Origins of Taiwan's mud volcanoes: Evidence from geochemistry, Journal of Asian Earth Sciences, 37 (2), 105-116, doi: 10.1016/j.jseaes.2009.02.007

Suppe, J. (1984), Kinematics of arc-continent collision, flipping of subduction, and back-arc spreading near Taiwan, Memoir of the Geological Society of China, 6, 21-33.

Suppe, J., C. D. Connors, and Y. Zhang (2004), Shear fault-bend folding, in K. R. McClay, ed., Thrust tectonics and hydrocarbon systems: AAPG Memoir 82, p. 303-323.

Tsai, M. C., S. B. Yu, T. C. Shin, K. W. Kuo, P. L. Leu, C. H. Chang, and M. Y. Ho (2015), Velocity field derived from Taiwan Continuous GPS Array (2007 - 2013), Terr. Atmos. Ocean. Sci., 26, 527-556, doi: 10.3319/TAO.2015.05.21.01(T)

Wei, M., D. Sandwell, Y. Fialko, and R. Bilham (2011), Slip on faults in the Imperial Valley triggered by the 4 April 2010 Mw 7.2 El Mayor-Cucapah earthquake revealed by InSAR, Geophys. Res. Lett., 38, L01308, doi:10.1029/2010GL045235.

Wessel, P., and W. Smith (1991), Free software helps map and display data, *Eos Trans. AGU*, *72*(441), 445-446.

Wright, T., E. Fielding, and B. Parsons (2001), Triggered slip: Observations of the 17 August 1999 Izmit (Turkey) Earthquake using radar interferometry. Geophys. Res. Lett., 28: 1079-1082. doi:10.1029/2000GL011776

Yu H.-L., H.-H. Shih, C.-S. Huang, C.-G. Ho, and B.-S. Tseng (1990), Geological review of the Lungchuan structure, Tainan and Kengnei, Shiaokunshui structure, Kaohsiung, Chinese Petroleum Corporation, R.O.C. [in Chinese]

Yuan, J., S.-T. Huang, T.-F. Chou, J.-C. Wu, D.-L. Lu (1987), The origin of the abnormal pressure zones in Southwestern Taiwan [in Chinese with English abstract], Ann. Explor. Prod. (CPC), 10, 1-27.